Imaging in Non-small Cell Lung Cancer

5

James G. Ravenel

Appropriate therapy is dependent on accurate staging to determine those amenable to surgery and define the appropriate role for chemotherapy and radiation therapy. In this chapter, the role of imaging in the staging and prognosis of lung cancer is discussed.

Chest Radiographs

Chest radiographs are typically the first studies performed in the evaluation of the patient with suspected lung cancer, although the paradigm may shift to a greater emphasis on CT as experience with screening CT increases. The typical radiographic finding is an irregular or spiculated nodule or mass, although border characteristics can vary and can be smooth or cavitary (Figs. 5.1–5.3). A second manifestation is collapse of a lobe owing to an endobronchial tumor (Fig. 5.4). The chest radiograph may also give evidence of mediastinal adenopathy or chest wall invasion. It is important to recognize that chest radiographs do not detect all lung tumors and that a negative radiograph in the setting of a high clinical suspicion should not necessarily end the radiographic evaluation. In addition, there are known "blind spots" on the radiographs particularly along mediastinal and hilar borders and beneath the rib and clavicular shadows (Fig. 5.5) [1].

J.G. Ravenel, M.D. (✉)
Department of Radiology, Medical University of South Carolina, 96 Jonathan Lucas St, Room 211, P. O. Box 250322, Charleston, SC 29425, USA
e-mail: ravenejg@musc.edu

CT, PET, and Histology

While on a practical basis for staging, the majority of primary lung cancers are grouped as either small cell or non-small cell lung carcinomas (NSCLC), the distinction of cell types in the NSCLC group is often of value in choosing certain treatment regimens. While this is truly the domain of pathology, certain imaging features may be present in the different histologic subtypes and may aid in diagnosis. While the classic teaching is that squamous cell carcinomas tend to be central and more likely to be cavitary than adenocarcinomas, there can certainly be overlap. One feature that appears to reliably predict adenocarcinoma as the histology is the presence of ground-glass opacity at CT [2] (Fig. 5.6). In the past, many of these tumors were grouped under the subtype bronchioloalveolar cell carcinoma (BAC), but owing to the confusion over terminology, these have been reclassified into in situ, minimally invasive and invasive adenocarcinoma to account for different biologic behavior and prognosis. Overall, the extent of ground-glass opacity appears to correlate with areas of hyperplasia, in situ carcinoma, or minimally invasive tumor which predicts slower growth and better overall prognosis [3–6]. Pure ground-glass nodules are typically atypical adenomatous

J.G. Ravenel (ed.), *Lung Cancer Imaging*, Contemporary Medical Imaging,
DOI 10.1007/978-1-60761-620-7_5, © Springer Science+Business Media New York 2013

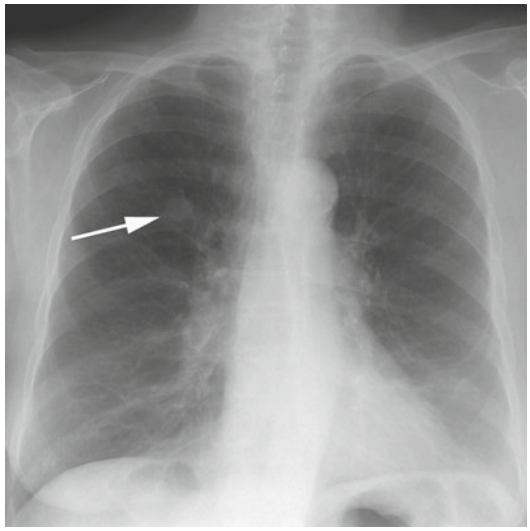

Fig. 5.1 Frontal chest radiograph reveals 2 cm right upper lobe solitary pulmonary nodule (*arrow*)

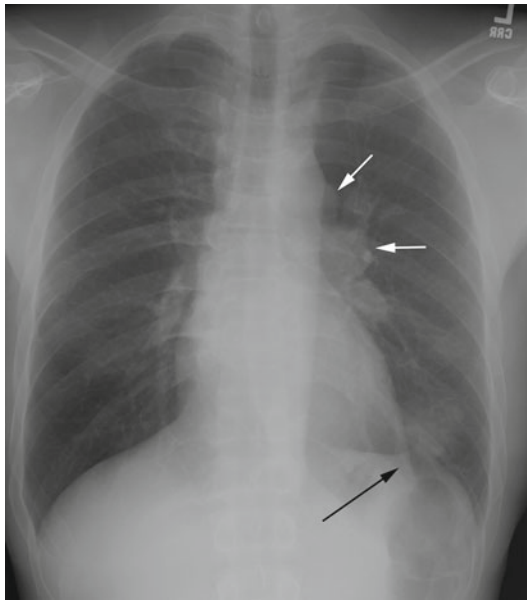

Fig. 5.2 Frontal chest radiograph reveals left lower lobe poorly defined nodule (*black arrow*) with associated left hilar and aortopulmonary window adenopathy (*white arrows*)

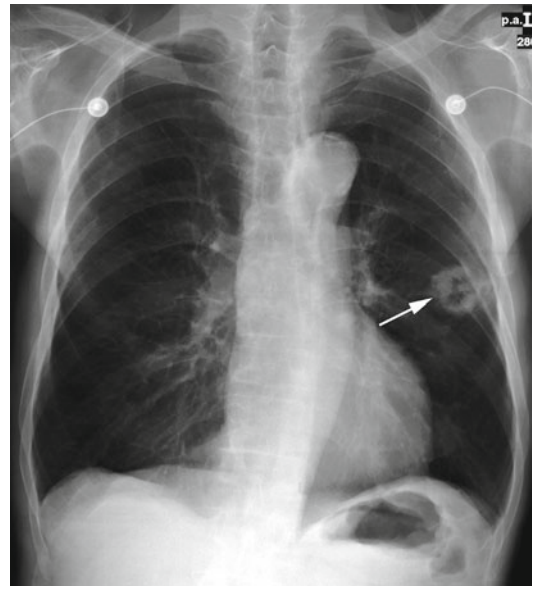

Fig. 5.3 Frontal chest radiograph reveals cavitary lung cancer in left upper lobe (*arrow*)

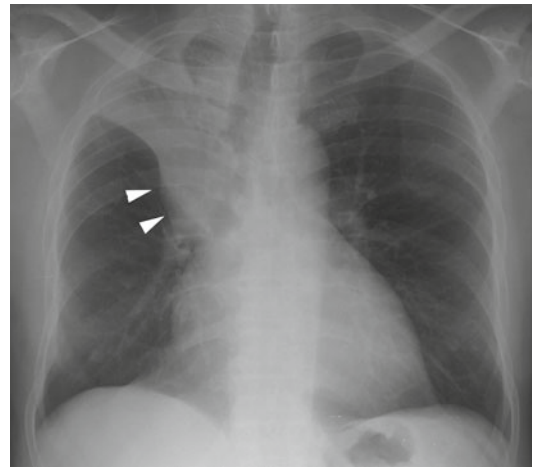

Fig. 5.4 Frontal chest radiograph reveals central right hilar mass (*arrowheads*) resulting in collapse of right upper lobe (also known as "S" sign of Golden)

hyperplasia or in situ adenocarcinomas but may on occasion contain an invasive component [7]. With FDG-PET, the standard uptake value tends to be higher with squamous and large cell histology [2], and similarly lung cancers that are not FDG avid are likely to be in the spectrum of low-grade adenocarcinoma [8–10].

The spectrum of low-grade adenocarcinoma is complex often requiring resection of the entire lesion to exclude an invasive component [11]. These tumors may present as a solitary pulmonary nodule or as diffuse confluent airspace

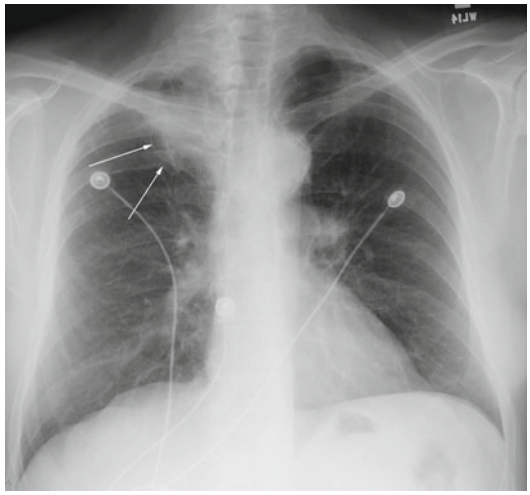

Fig. 5.5 Frontal chest radiograph reveals density differences between right (*arrows*) and left lung apices, although exact borders of mass are hard to define

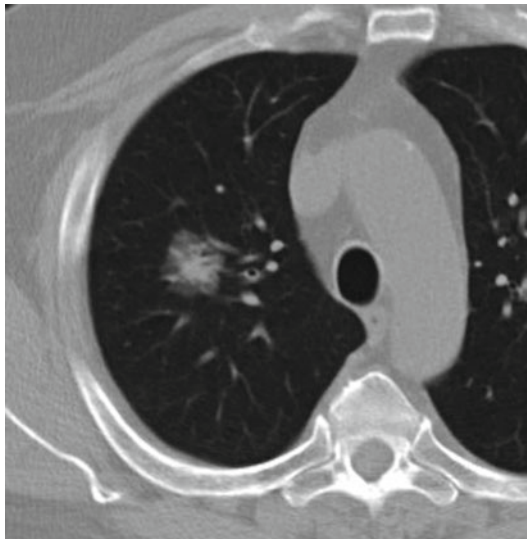

Fig. 5.6 Axial CT image reveals part-solid nodule with solid core and peripheral ground-glass opacity. Appearance is typical of invasive adenocarcinoma

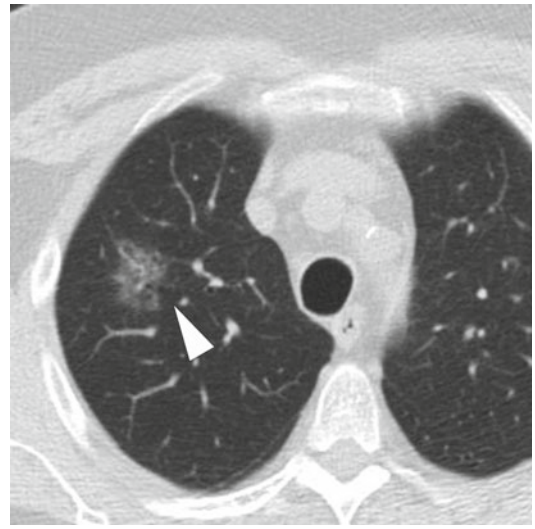

Fig. 5.7 Axial CT image reveals a pure ground-glass nodule with associated irregular borders air bronchograms and bubble-like lucencies (*arrowhead*) features often associate with preinvasive or minimally invasive histologies

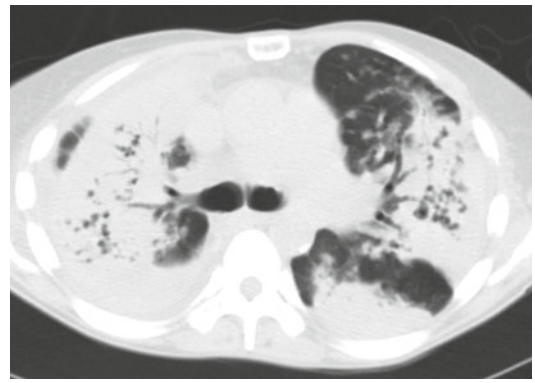

Fig. 5.8 Axial CT image reveals widespread parenchymal consolidation with pseudocavitation. Bronchoscopy revealed multifocal mucinous adenocarcinoma

disease. Nodules may have a variety of appearances including lobulated or spiculated borders, pleural tags, air bronchograms, and internal lucencies (pseudocavitation) [12] (Fig. 5.7). The ground-glass opacity histologically reflects the lepidic tumor growth with or without alveolar collapse [9], while the lucencies presumably reflect either uninvolved lobules or focal air trapping with bronchiolar obstruction [13, 14]. While a solid component may simply reflect alveolar collapse, it is more likely to represent areas of fibroblast proliferation or invasive adenocarcinoma [15].

A second radiographic appearance is the diffuse or multifocal form (Fig. 5.8). Findings range from multiple ground-glass opacities and nodules to lobar consolidation [12]. In many cases, the

initial distinction from infection is impossible and the disease is not considered until the "pneumonia" does not resolve. The filling of airspaces is generally the result of mucin production, and with contrast-enhanced CT the underlying architecture of the lung is preserved. Sufficient mucin may eventually lead to attenuation of the pulmonary vessels and a bulging fissure [16]. The finding of discrete nodules in other lobes combined with non-resolving consolidation strongly supports the diagnosis [17]. The CT angiogram sign reflects normal pulmonary vasculature coursing through consolidated lung and can be seen in cases of infection, lipoid pneumonia, and obstructive pneumonitis [18].

NSCLC Staging

CT allows for anatomic staging of the primary lesion, mediastinal lymph nodes, and distant metastatic disease. The major limitations of anatomic imaging are the use of size criteria to define benign versus malignant lymph nodes, failure to distinguish tumor from atelectasis, and the nonspecific appearance of metastatic disease in general. The addition of metabolic imaging (FDG-PET) adds sensitivity and specificity to staging but does not replace histologic confirmation.

Staging is categorized by the TNM system, which is accepted by the American Joint Committee on Cancer (AJCC) [19]. This classification system takes into account the primary lesion (T), the presence or absence of mediastinal or supraclavicular lymph node involvement (N), and the presence or absence of distant metastasis (M) (Tables 5.1 and 5.2).

Table 5.1 Staging of lung cancer: AJCC TNM descriptors

Primary lesion
T0-no evidence of primary tumor
Tis-carcinoma in situ
T1-tumor <3 cm surrounded by lung or visceral pleura without invasion proximal to lobar bronchus
1a- ≤2 cm
1b- >2–3 cm
T2-tumors >3 cm, any tumor invading main bronchi but >2 cm from the carina, invasion of visceral pleura, obstructive pneumonitis extending to hila but does not involve entire lung
2a- >3–5 cm
2b- >5–7 cm
T3-tumor >7 cm. Tumor of any size that directly invades chest wall, diaphragm, mediastinal pleura, or parietal pericardium; or involves main bronchus within 2 cm of carina but does not involve carina; or results in obstructive atelectasis or pneumonitis of entire lung. Separate nodule(s) in same lobe
T4-tumor invades any of the following: mediastinum, heart great vessels, trachea, esophagus, vertebral body, or carina; malignant ipsilateral pleural or pericardial effusion; separate nodule(s) in a different ipsilateral lobe
Lymph nodes
N0-no regional lymph node metastases
N1-spread to ipsilateral peribronchial or hilar nodes
N2-spread to ipsilateral mediastinal or subcarinal nodes
N3-spread to contralateral mediastinal or hilar nodes, scalene nodes, supraclavicular nodes
Distant disease
M0-no distant metastases
M1-distant metastases present
M1a-separate tumor nodule in contralateral lung, pleural nodules, malignant pleural, or pericardial effusion
M1b-all other distant metastasis

T-Stage

The evaluation of T-stage is based upon size and location of the lesion, commonly using CT. The use of intravenous (IV) contrast while often specified in clinical trials is not mandatory as no clear superiority of contrast-enhanced CT scans has been established [20–22]. The use of IV contrast is therefore best left to the discretion of the interpreting physician.

T1 tumors are those that are less than 3 cm in greatest dimension and that do not invade the visceral pleura or mainstem bronchi. These can be further subdivided into T1a (<2 cm) and T1b (≥2 cm <3 cm) (Fig. 5.9). T2 tumors are greater

Table 5.2 Staging of NSCLC based on TNM classification

0-	Carcinoma in situ
1A-	T1N0M0
1B-	T2aN0M0
2A-	T2bN0M0
	T1N1M0
	T2aN1M0
2B-	T2bN1M0
	T3N0M0
3A-	T3N1M0
	T1-3N2M0
	T4N0-1 M0
3B-	T4N2M0
	Any N3
4-	Any M1

Used with the permission of the American Joint Committee on Cancer (AJCC), Chicago, Illinois. The original source for this material is the *AJCC Cancer Staging Manual*, Seventh Edition (2010) published by Springer Science and Business Media LLC. http://www.springer.com

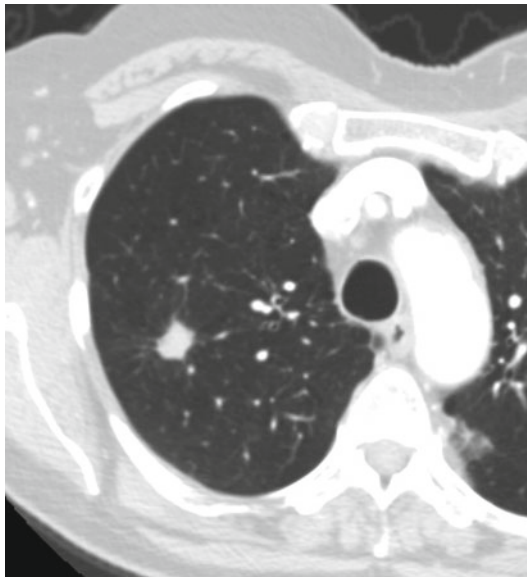

Fig. 5.9 T1 lesion. Axial CT image reveals a 1.4 cm spiculated right upper lobe nodule typical for lung neoplasm

than 3 cm and <7 cm in greatest dimension and/or involve the visceral pleura or mainstem bronchi, at least 2 cm from the carina (Fig. 5.10). T2 tumors can be subdivided into a and b categories based on whether tumor size is less than or

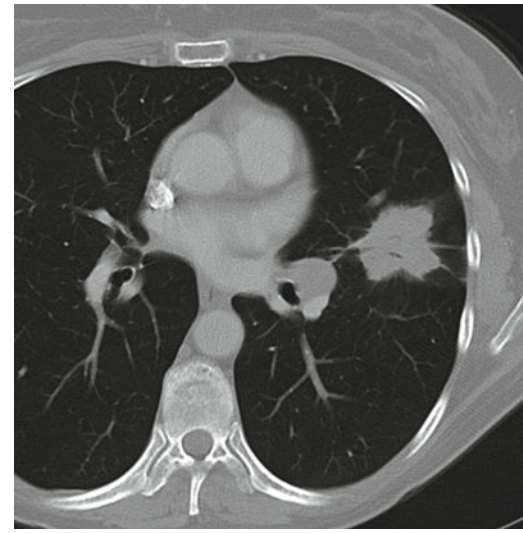

Fig. 5.10 T2 lesion. Axial CT image reveals a 4 cm spiculated mass in the left upper lobe

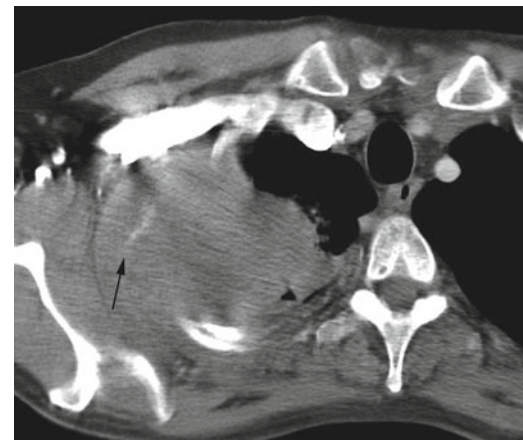

Fig. 5.11 T3 lesion. Axial CT reveals large right upper lobe mass with invasion into chest wall and destruction of right second rib (*arrow*)

greater than 5 cm. Regardless of size, it is important to note the relationship of the tumor to the pulmonary artery, lobar fissures, and incomplete fissures when applicable as this may alter the planned surgical approach [23]. T3 tumors include those ≥7 cm, are of any size that involve the chest wall, diaphragm, mediastinal pleura, parietal pericardium, or are within 2 cm of the carina but do not invade the carina (Fig. 5.11). Satellite nodules in the same tumor lobe are also

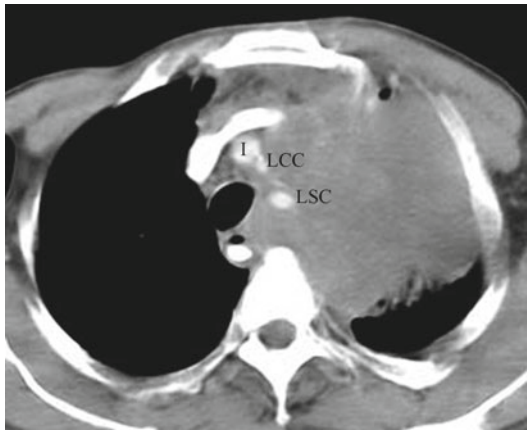

Fig. 5.12 T4 lesion. Axial CT reveals large left upper mass with invasion into the mediastinum and encasement of the innominate artery (I), left common carotid artery (LCC), and left subclavian artery (LSC)

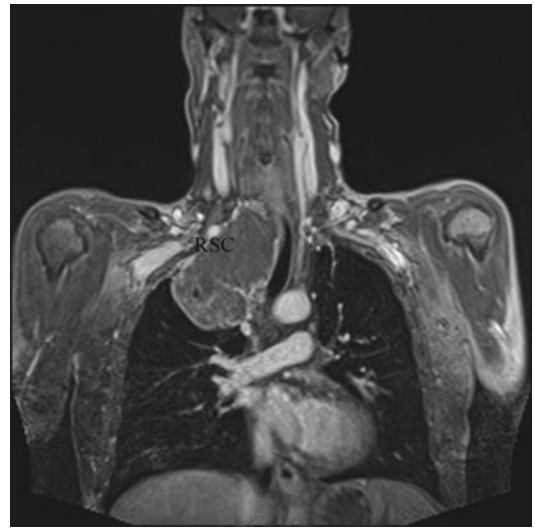

Fig. 5.13 Pancoast tumor. Coronal gadolinium-enhanced T1 sequence reveals cephalad extension of superior sulcus tumor, abutting the right subclavian artery (RSC)

considered T3 tumors regardless of the size of the dominant nodule/mass. T4 tumors invade vital structures including the heart, great vessels, esophagus, carina, or vertebral body or contain a satellite nodule in the ipsilateral lung non-tumor lobe (Fig. 5.12). While T4 tumors are generally considered unresectable, in certain circumstances, complete surgical resection may be feasible [23].

The distinction between T1 and T2 tumors is generally straightforward and does not usually impact initial treatment. Difficulty with T-staging may arise when there is need to determine chest wall (T3) or mediastinal (T4) invasion. Whereas primary signs such as bone destruction, rib erosion, or the presence of a tumor adjacent to mediastinal structures are reliable evidence of invasion, secondary signs such as absent fat planes, pleural thickening, and obtuse angle of tumor contact with the chest wall are not reliable [24–26]. Several CT features have been described to help determine chest wall invasion. These include greater than 3 cm of contact with the pleural surface, pleural thickening, absent fat planes, and obtuse angle of tumor with the chest wall [26]. Although sensitivity is relatively good with at least two features present (87 %), specificity remains relatively low (59 %), and localized chest pain remains a much more specific determinant [26]. Using thinner collimation with coronal and sagittal reformation improves accuracy for both chest wall and mediastinal invasion [27].

Magnetic resonance (MR) imaging can aid in problem solving and is clearly better at delineating extension of superior sulcus tumors [28]. In particular MR is superior to CT for the detection of involvement of the neural foramina, spinal canal, and brachial plexus. Surgery is contraindicated by local extension when the brachial plexus is involved above the level of T1, more than 50 % of a vertebral is invaded, or when there is invasion of the trachea or esophagus (Fig. 5.13). Invasion of the subclavian, common carotid, and vertebral arteries, less than 50 % vertebral body invasion and extension into the neural foramina, should be considered relative contraindications to surgery [28]. In other cases, the tumor should be considered a T3 lesion and treatment decisions should be based on the patient's medical condition as well as the presence or absence of metastatic disease.

MR can also be useful in excluding chest wall involvement. Using cine MR during free breathing, the finding of sliding between the tumor and mediastinum or chest wall has been shown to be diagnostic of lack of invasion. The converse

however is not necessarily indicative of invasion as adhesion and local inflammatory changes may also restrict tumor motion [29–31].

In the appropriate hands, ultrasound also can be a useful adjunct in detecting chest wall invasion. In several studies, ultrasound has been shown to be superior to CT with sensitivity greater than 90 % [32, 33]. Sonographic features of chest wall invasion include direct invasion of the chest wall, interruption of the pleural reflection, and impairment of motion with respiration [32]. Ultrasound may be limited in certain circumstances, and false-negative and false-positive results may be obtained due to shadowing from osseous structures or fibrous adhesions of the tumor to pleura, respectively. Endoscopic ultrasound can also be utilized to assess mediastinal and aortic invasion [34, 35]. Because it is a relatively untested technique in this setting, the actual utility will depend on operator technique and experience.

PET/CT and T-Staging System

Due to the limited spatial resolution, 18F-FDG PET does not have a specific role in staging the primary tumor. While it has been suggested that fusion of CT and 18F-FDG PET images together may enhance T-stage determination (particularly for chest wall and mediastinal invasion) [36], care must be taken not to over- or under-stage tumors due to respiratory misregistration. By acquiring CT images at medium lung volumes rather than at deep inspiration, misregistration problems can be minimized. However, careful analysis of the CT images without 18F-FDG PET is still mandatory in order to avoid this pitfall. In rare circumstances, 18F-FDG PET may be helpful in detecting an occult primary tumor suspected based on detection of distant metastases.

Prognosis by PET/CT

As already seen, size and local invasion are predictors of survival at CT. FDG PET and PET/CT can also be used to evaluate long-term prognosis.

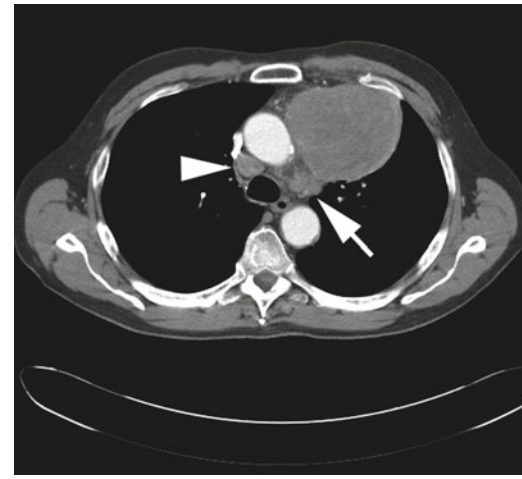

Fig. 5.14 Mediastinal adenopathy. Left upper lobe neoplasm with ipsilateral (N2) aortopulmonary adenopathy (*arrow*) and contralateral right paratracheal (N3) adenopathy (*arrowhead*)

In a retrospective study, 2-year survival was 96 % for surgically treated patients with an SUVmax <9 and 68 % if >9. The combination of tumor size >3 cm and SUVmax >9 resulted in only 47 % survival at 3 years [37]. However, when adjusting for surgical pathologic stage, SUVmax did not predict prognosis [38]. Other investigators have proposed a cutoff of SUVmax of 5–5.5 and found a survival advantage in the low SUV group [39–42]. This survival advantage was also supported by a recent meta-analysis showing that high SUV tumors were associated with reduced survival and a hazard ratio of 2.07 [43]. Unlike size, however, the use of SUV has not been included in the staging system and presumably reflects the variability in SUV across sites and scanners as well as the lack of an agreed upon measurement standard.

N-Stage

N-stage is defined by the presence or absence of lymphadenopathy and the relationship of the abnormal lymph nodes to the primary tumor (Fig. 5.14). Nodal location is defined by the IASLC lymph node map [44] (Fig. 5.15). N1 is defined as nodes which are ipsilateral intrapulmonary, peribronchial, and hilar. N2 nodes are ipsilateral mediastinal nodes, including the midline groups

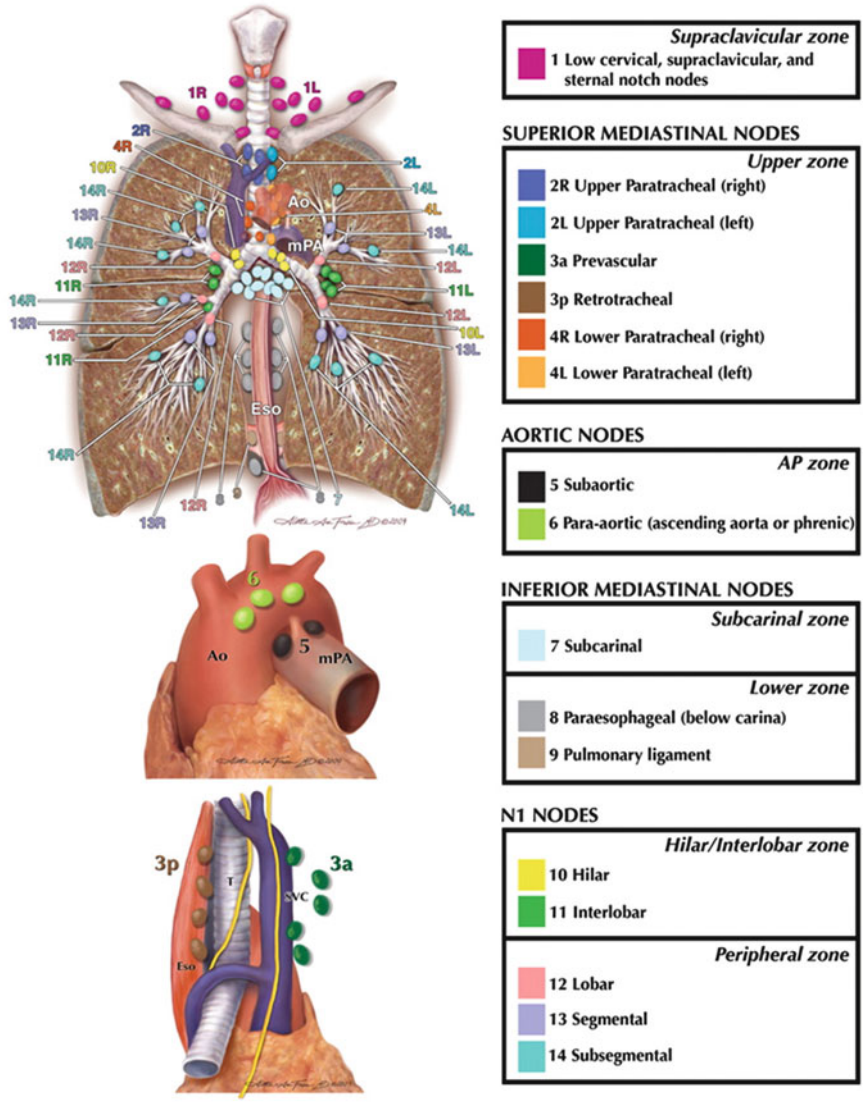

Fig. 5.15 IASLC lymph node map

(levels 3 and 7). Finally, N3 nodes are contralateral to the primary tumor or involve the scalene or supraclavicular nodes. The location of the primary tumor has a strong and relatively predictable influence on the likely location of metastatic nodes. Right upper lobe tumors most often drain to right paratracheal nodes (2R and 4R), while right middle and lower lobe tumors most frequently drain to lower right paratracheal and subcarinal nodes (4R and 7). On the left, the common sites for nodal metastases for the left upper lobe include AP window and prevascular nodes (5 and 6) and prevascular and subcarinal (6 and 7) for the left lower lobe [45]. For lower lobe tumors, the frequency of upper mediastinal lymph node involvement (levels 2, 4, 5, 6) is greater for tumors in the superior segment (64 %) versus basal segments (36 %) [46]. Because size is the main criteria for malignancy, CT is relatively inaccurate for staging the mediastinum. A lymph node measuring greater than 1 cm in short axis diameter is generally considered "positive" for clinical

Fig. 5.16 T1N2 lung cancer. Composite of PET/CT reveals right upper lobe spiculated nodule with 1 cm borderline enlarged right paratracheal lymph node with FDG activity. Confirmed as lymph node metastasis by endobronchial ultrasound and biopsy

staging purposes [47]. While there is no lower limit of size that guarantees freedom from disease, the overall chance that a node is malignant is clearly influenced by size. For example, the prevalence of metastatic disease in lymph nodes is approximately 30 % for nodes 10–15 mm in size and 67 % for nodes >15 mm in size [48]. Among 43 studies conducted from 1991 to 2005, the sensitivities of CT for nodal disease ranged from 26 to 86 % and specificity ranged from 31 to 97 % with a pooled sensitivity and specificity from a total of 5,111 patients in whom prevalence of nodal disease was 28 % of 51/86 % [49]. CT, most importantly, provides anatomic relationships and landmarks critical for interpreting 18F-FDG PET studies and allows for selection of the most appropriate pathway for biopsy.

18F-FDG PET improves noninvasive staging but is not a substitute for tissue. Pooling all studies resulted in sensitivity/specificity of 74 %/85 % 2,865 patients with a prevalence of mediastinal disease of 29 % [49]. A prior meta-analysis showed a sensitivity and specificity of 85 %/90 % [50], suggesting that with more widespread acceptance and utilization, the true test characteristics are not as good as once thought. While 18F-FDG PET is not an endpoint in the staging work-up, 18F-FDG PET scans can decrease the number of futile thoracotomies by 20 % [51, 52]. The PLUS study [51] randomized stage I–III patients who were potentially operable to FDG PET or no PET and showed a reduction in the "futile" thoracotomy rate (thoracotomy performed in patients with unresectable disease) by 20 % (41 % without 18F-FDG PET vs. 21 % with 18F-FDG PET). However, for clinical 1A patients, the yield of 18F-FDG PET in preventing nontherapeutic pulmonary resection appears to be less than 10 % [53]. Thus, the ultimate success of 18F-FDG PET in the mediastinum may be to spare advanced-stage patients extensive surgery.

It is clear that 18F-FDG PET must be interpreted in the context of CT findings to maximize utility, and the value of 18F-FDG PET in staging the mediastinum is dependent on the CT findings [50, 54]. If a CT contains enlarged lymph nodes greater than 1 cm, sensitivity of 18F-FDG PET approaches 100 %, but specificity decreases (~78 %). In the setting of a negative CT scan, 18F-FDG PET shows lower sensitivity (82 %) but improved specificity (93 %) (Fig. 5.16) [50]. Modeling for size in combination with PET the likelihood of malignancy in a PET-negative node is 5 % when 10–15 mm in size and 21 % when greater than 15 mm in size. Conversely, the likelihood of malignancy in a PET-positive node is 62 % when 10–15 mm and 90 % when >15 mm [48].

The relationship of nodal SUV to malignancy is similar to that of size; the overall likelihood of malignancy increases with increasing SUV. Although a wide range of maximum SUV can be associated with benignity, accuracy improves with an SUV > 5.3 [55]. Additionally, the true positive rate is higher in lymph nodes <1 cm with elevated SUV [56].

The ratio of SUV of the mediastinal lymph nodes to the primary tumor can also be helpful. A ratio of 0.56 predicted malignancy with a sensitivity of 94 % and specificity of 72 %, but like SUV alone, showed extensive overlap between

benign and malignant lymph nodes [57]. The reality is that 18F-FDG PET should not replace histologic staging in the vast majority of cases. Most notably, a single positive finding should always be confirmed by histology before considering as stage 3 disease.

In regard to the 18F-FDG PET-negative mediastinum, there appear to be several caveats that can guide whether further mediastinal staging is necessary. A retrospective study of 18F-FDG false-negative results found that occult metastases were more likely to occur with increasing T-stage, central tumors, adenocarcinoma histology, and higher primary tumor SUV (>6), although the actual number of false-negative lymph nodes in this study was small ($n=16$) [58]. Other groups have found that in addition to these features, upper lobe tumors and those with N1-positive disease also have a relatively high rate of occult disease in the mediastinum with histologic staging [59, 60]. The size of false-negative lymph nodes tends to be less than 1 cm; therefore, while the negative predictive value of the PET-negative mediastinum is quite high, the potential for a false-negative result is associated with decreasing node size. Tobacco use appears to lower maximum SUV and both smoking status and maximum pack years are independently associated with a decreased accuracy of 18F-FDG PET for mediastinal staging [61]. In summary, an 18F-FDG PET-negative mediastinum has an extremely high negative predictive value in small (T1), peripheral tumors with a low primary tumor SUV and no significant activity in the hilar lymph nodes. Under these conditions, it seems reasonable to proceed to surgery without prior pathological staging of the mediastinum.

Integrated 18F-FDG PET/CT imaging outperforms CT alone, 18F-FDG PET alone, and conventional visual correlation or superimposition of CT and 18F-FDG PET acquired individually [36, 62–64]. The diagnostic advantages touted in the literature include more precise demarcation of primary tumor (which can also be used to better define radiation ports), improved diagnosis of tumor invasion, demarcation of tumor within atelectasis or infection, more precise localization of mediastinal lymph nodes greater than 8 mm in size, as well as the precise localization of extrathoracic lesions [65]. Most notably, integrated systems allow more accurate staging impacting treatment decisions in up to 20 % of patients [62].

MR imaging is not typically used for mediastinal staging, although abnormal lymph nodes can be detected using this technique. A lack of standardization of protocols however makes comparison of results difficult. Most protocols utilize a short tau inversion recovery (STIR) sequence which allows for whole-body staging with a total exam time of 60 min [66]. Using this approach, MR imaging approaches the accuracy of PET/CT for detecting nodal metastases at 1.5 T [67]. A slightly shorter imaging time is feasible with 3.0 T MR and likewise has relatively similar, albeit slightly less accurate [68]. In one study STIR images using quantitative analysis using a lymph node-saline ratio were found to be more sensitive and specific compared to PET/CT [69].

Owing to the increased cellularity, larger nuclear size, and decreased extracellular space, the motion of water molecules is restricted. One attempt to improve evaluation with MR is the addition of diffusion-weighted imaging (DWI) to evaluate the apparent diffusion coefficient (ADC). The results, however, have been mixed. Ohno et al. evaluated 250 consecutive patients with T1 or T2 NSCLC using a STIR sequence, DWI, and FDG PET/CT and found STIR images to be slightly more accurate than either DWI or FDG PET/CT [70]. In a smaller study of 63 subjects, Usada et al. found DWI to be superior in detecting both primary tumor and lymph node metastasis [71]. Pauls et al. were unable to demonstrate an advantage of DWI over FDG-PET and noted that MR had a greater tendency to understage patients [72]. DWI may improve delineation of central tumors from post-obstructive pneumonitis [73]. It is clear that MR imaging can be used to stage lung cancer with similar test characteristics to standard techniques but requires agreement on the optimal technique and validation in a multicenter trial.

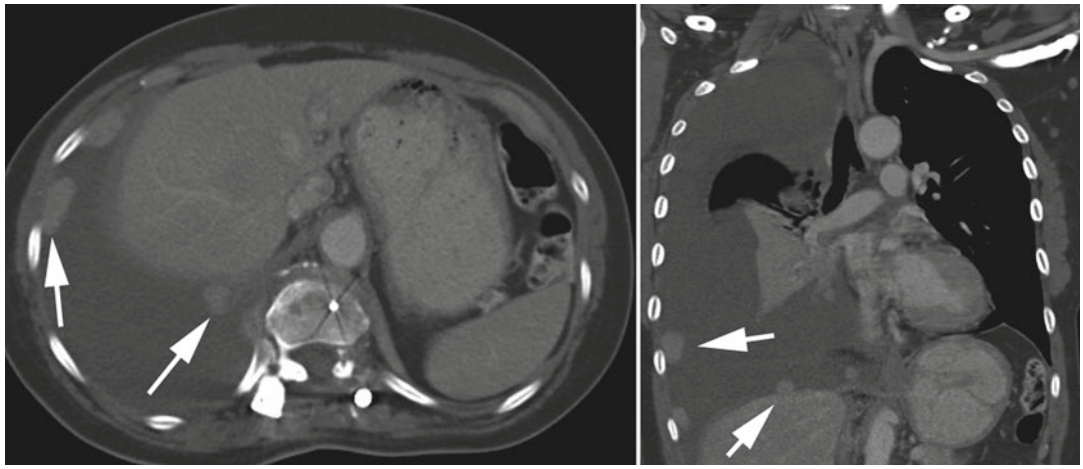

Fig. 5.17 Pleural metastases. Axial and coronal CT images reveal large right pleural effusion with enhancing pleural nodules (*arrows*)

M-Stage

M-stage is defined by the absence (M0) or presence (M1) of distant metastasis. The M-category is further subdivided into M1a-malignant pleural effusion and M1b-other distant metastases. Lung cancer most commonly metastasizes to bone, brain, liver, and adrenal glands. CT and whole-body 18F-FDG PET imaging are usually used for the evaluation of distant metastases. In the absence of symptoms, the negative predictive value is usually 95 % for liver, brain, and adrenal and 90 % for bone [74, 75]. Whole-body MR imaging as discussed previously also has the capability of providing accurate staging in a single exam. In limited studies, whole-body MR is as accurate as 18F-FDG PET in detecting distant metastases and seems to have a particular advantage in detecting brain and liver lesions [68]. The addition of diffusion-weighted images may ultimately increase yield [76].

Pleural Metastasis

Ipsilateral malignant pleural effusions are considered to be M1a by staging criteria and are most frequently associated with adenocarcinoma histology. However, pleural effusions are not uncommon in patients with lung cancer and are not necessarily due to the presence of malignant disease in the pleural space. Malignant pleural effusions by definition have tumor cells in the pleural space and almost always exudates (3–10 % will be transudates) [77]. In some cases the effusions are paramalignant due to central venous or lymphatic obstruction or effusions due to post-obstructive atelectasis/pneumonitis [78]. Effusions in lung cancer patients may also result unrelated to the tumor itself (cardiac, hepatic, renal disease, etc.), thus sampling of the fluid is mandatory prior to labeling a patient unresectable. CT findings suggesting a malignant effusion include parietal pleural thickness >1 cm, circumferential thickening, and nodules and mediastinal pleural involvement (Fig. 5.17) [77]. 18F-FDG PET has been shown to be quite accurate (>90 %) in the confirmation of metastatic pleural disease in two series [79, 80].

Adrenal Metastasis

Adrenal nodules are a common incidental finding in the general population and in patients with lung cancer (Fig. 5.17). The majority of these lesions represent benign adenomas. In this case, unenhanced CT holds an advantage over contrast-enhanced CT, as a density measurement of <10 HU virtually assures the diagnosis of benign adenoma [81]. The low attenuation is due to intracellular lipid accumulation within benign lesions. However, a number of adrenal lesions have a density >10 HU and are considered indeterminate.

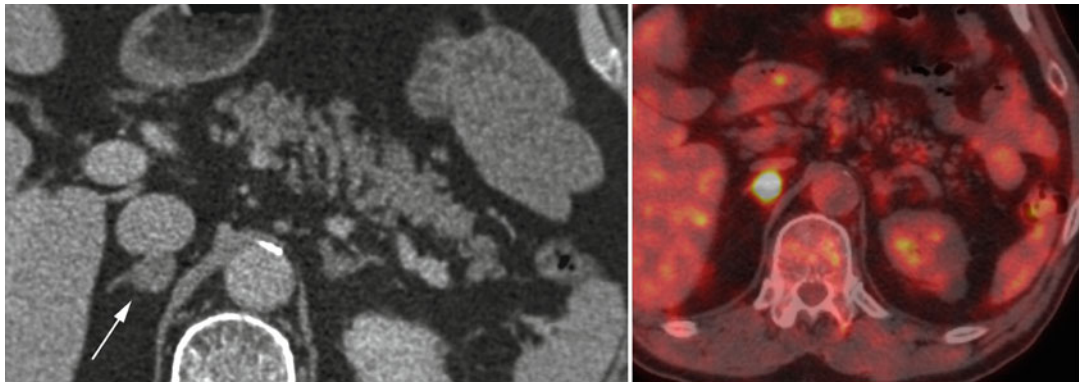

Fig. 5.18 Indeterminate adrenal lesion (*arrow*). Axial CT and fused PET/CT images reveal a metabolically active right adrenal nodule. Because this was only potential site of metastatic disease, biopsy was performed and revealed nonfunctioning pheochromocytoma

Similarly, on contrast-enhanced CT, both benign and malignant lesions invariably exceed the threshold of 10 HU. If an adrenal lesion is recognized after contrast administration, but prior to leaving the scanner, a delayed washout technique can be employed to distinguish benign and malignant lesions. If greater than 50 % of the attenuation "washes out" after 15 min, the lesion is an adenoma [82, 83]. For indeterminate lesion on unenhanced CT, histogram analysis can also improve sensitivity. If the lesion has >10 % pixels with a negative HU value, it is invariably a benign adenoma. This technique appears to be able to characterize indeterminate adrenal lesions as benign lipid-poor adenomas in approximately ½ of cases [84–86]. This technique can also help characterize lesions that remain indeterminate after washout studies [87].

MR imaging with in-phase and out-of-phase sequences is an alternative to CT. Signal dropout can be used to reliably confirm the benign nature of an incidental adrenal lesion [88]. While it has been suggested that MR is of limited utility when CT attenuation values are >10 [89, 90], it can be a useful strategy for following up lesions detected on contrast-enhanced scan without using additional contrast media, and in one study signal intensity dropout of >20 % performed better than histogram analysis at CT [85].

18F-FDG PET has been shown to differentiate benign and malignant adrenal lesions, even those indeterminate at CT and MR, with a sensitivity and specificity of 94–100 % and 74–91 % in a total of four studies [91–94]. The most important observation is that benign nodules can be FDG avid, and therefore PET activity in the adrenal gland should not necessarily confirm a patient as stage IV disease (Fig. 5.18).

Liver Metastasis

The most common hepatic lesions detected by CT in the evaluation of lung cancer are benign cysts or hemangiomas. Given the frequency of indeterminate findings, it is reassuring that the liver is rarely the sole site of metastatic disease at time of diagnosis, occurring in approximately 3 % of cases [95]. As most chest CT scans will cover the majority of the liver, dedicated hepatic imaging is generally not indicated. While this suggests a benefit to enhanced CT for staging, careful evaluation of the unenhanced CT with narrow window settings will allow for visualization of most hepatic metastases. In cases where differentiation of benign and malignant lesion is necessary, MR can often be definitive in distinguishing the two (Fig. 5.19). 18F-FDG PET has not been formally evaluated for imaging of liver metastasis related to lung cancer; however, experience in other malignancies suggests that 18F-FDG PET can accurately detect liver metastases by focal uptake greater than the background of the liver [96].

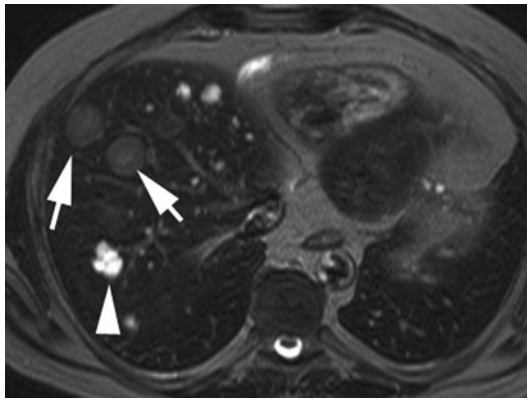

Fig. 5.19 Liver metastases and cysts. T2-weighted axial MR in patients noted to have multiple hypointense lesions on CT. MR clearly distinguishes the marked high signal in cysts (*arrowhead*) and differentiates them from metastatic lesions (*arrows*)

Bone Metastasis

Most patients with bone metastases are symptomatic or have an elevated alkaline phosphatase. While bone scintigraphy is quite sensitive for the detection of osseous metastases, the false-positive rate approaches 40 %. Since fewer than 5 % of lung cancer patients have occult bone metastases at presentation [97], routine bone scintigraphy is probably not warranted. Bone scintigraphy, the current standard for osseous metastases, suffers from a relatively low specificity.

Routine CT allows for evaluation of the thoracic spine, upper lumbar spine, scapula, and ribs. While CT is not thought of as a modality for the detection of bone metastases, careful evaluation of osseous structures, with an appropriate window and level setting, frequently allows for the detection of metastases, particularly when correlated with either bone scintigraphy or 18F-FDG PET. In particular, using CT in this manner may limit false-positive studies by confirming degenerative changes as a cause of increased uptake on bone scintigraphy. Bone metastases may appear as lytic or destructive lesions or as regional areas of sclerosis (Fig. 5.12). In some cases, CT may in fact be the first clue to the presence of osseous metastasis.

Several studies have shown 18F-FDG PET to have a similar sensitivity and accuracy, with improved specificity and negative predictive value [98–100]. Thus, if whole-body 18F-FDG PET has already been performed, bone scintigraphy is usually superfluous (Fig. 5.20).

Brain Metastasis

CT with contrast is accurate for the detection of cerebral metastasis, although MR performance characteristics are slightly better (Fig. 5.21) [101]. Not surprisingly, the incidence of brain metastasis also increases with increasing size of the primary lesion and nodal stage [102]. However, in the absence of neurological symptoms, cerebral metastases are unusual and the routine staging of subjects with a normal clinical exam yields positive findings in less than 10 % [103–105]. Of the various histologic subtypes, adenocarcinoma and large cell carcinoma are most frequently associated with asymptomatic cerebral metastases [106]. Cerebral imaging is therefore most efficaciously utilized in patients with neurologic symptoms or prior to resection of T2 tumors or planned resection of IIIA disease. 18F-FDG PET has relatively low sensitivity and is not a suitable modality for the evaluation of metastatic disease, due to the brain's high metabolic activity and glucose consumption [107].

New Frontiers/Novel Imaging Techniques

Although clinical practice standards are generally guided by the concepts previously outlined, newer techniques for imaging are emerging and in a relative infancy of use. Whether any of these techniques improve on current staging and treatment algorithms, remain niche techniques for specific clinical questions or fall by the wayside remain to be seen. Several potential approaches are briefly discussed below.

Perfusion CT

CT perfusion is based on the theory that iodine maps are a surrogate for tumor vascularity. The evaluation of lung tumors with perfusion CT is

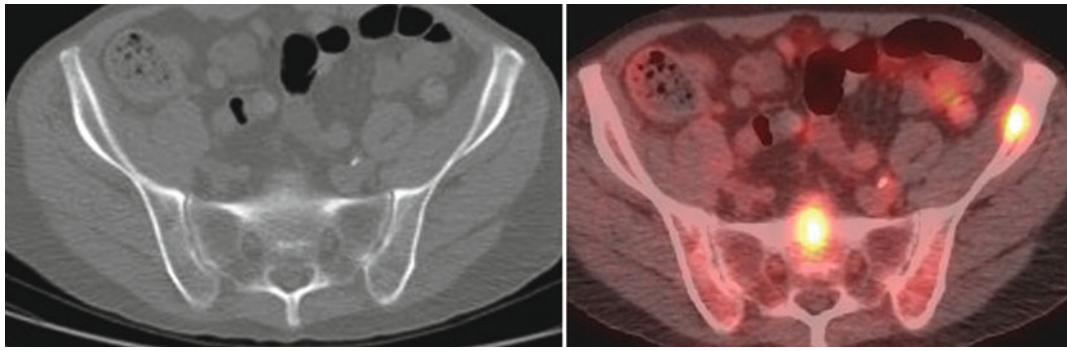

Fig. 5.20 Bone marrow metastases. Axial CT and fused PET/CT image show foci of FDG uptake in sacrum and left ilium with evidence of bone erosion or destruction. Such lesions can be occult on bone scintigraphy due to lack of bone remodeling

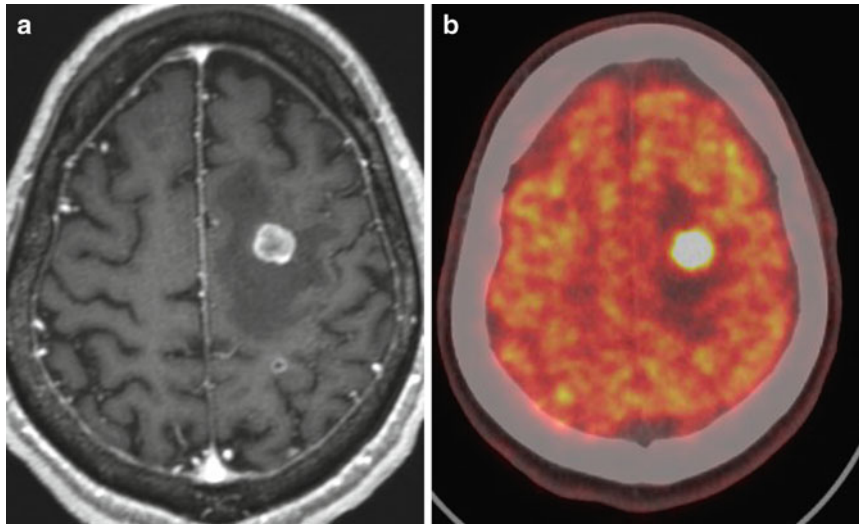

Fig. 5.21 Brain metastasis. (**a**) Axial gadolinium-enhanced MR reveals enhancing left parietal metastasis with surrounding vasogenic edema. (**b**) Axial 4-h delayed time point fused FDG PET/CT reveals metabolic activity above background. The activity is often masked at the time of the whole-body PET acquisition

challenging owing to a long imaging time and therefore long breathhold compared with static regions such as rectal and head and neck tumors where perfusion CT has been more widely studied. A recent small study in lung tumors has suggested that an increase in tumor blood volume is associated with better prognosis and that changes in permeability during therapy (decrease in permeability correlates with improved survival) can also predict outcome [108]. Another potential use is detecting a response to anti-angiogenic therapy where perfusion changes may be more predictive than size [109].

Positron Agents

Imaging Tumor Proliferation-18F-Fluorothymidime (FLT-PET)

Alternative imaging approaches to response may be evaluated by assessment of cellular proliferation. In theory the use of proliferation may lead to a better prediction of tumor behavior than metabolism. Proof of concept for FLT-PET has been shown similar to FDG-PET in subjects treated with gefitinib where time to progression was longer for responders compared to nonresponders [110]. A similar proof of concept showed that

FLT-PET can be used in tracking response to radiation therapy, although the significance of response was not evaluated [111]. However, in small studies FLT-PET does not appear superior to FDG-PET. In a study of 18 subjects with NSCLC, FLT had and lower mean SUV and a lower sensitivity than FDG, nor was it superior to FDG with regard to correlation with Ki-67 proliferation index [112]. FLT also has a tendency to understage patients owing to its relatively lower SUV compared with FDG [113]. A major limitation of these studies is that they do not address whole-body staging. Because of uptake in the liver, FLT is unreliable for the detection of liver metastases due to high physiologic activity and limits its potential as a staging agent [114].

Imaging Tumor Hypoxia-18F-Fluoromisonidazole (F-MISO)

Another approach is to assess tissue hypoxia. F-MISO is the most widely studied PET agent for tissue hypoxia [115]. Higher levels of hypoxia are predictive of poor local and distant control, and F-MISO appears to be a better predictor of outcome compared with FDG-PET in head and neck cancers [116] and perhaps for lung cancer.

Conclusion

Imaging plays a critical role in staging patients with non-small cell lung cancer. While mediastinoscopy is still considered the gold standard in mediastinal staging, imaging is beneficial in that it is noninvasive and highly accurate, especially when anatomic and physiologic information is acquired simultaneously through integrated 18F-FDG PET/CT systems.

References

1. Woodring JH. Pitfalls in the radiologic diagnosis of lung cancer. AJR Am J Roentgenol. 1990;154(6):1165–75.
2. Aquino SL, Halpern EF, Kuester LB, Fischman AJ. FDG-PET and CT features of non-small cell lung cancer based on tumor type. Int J Mol Med. 2007;19(3):495–9.
3. Aoki T, Nakata H, Watanabe H, et al. Evolution of peripheral lung adenocarcinomas: CT findings correlated with histology and tumor doubling time. AJR Am J Roentgenol. 2000;174(3):763–8.
4. Aoki T, Tomoda Y, Watanabe H, et al. Peripheral lung adenocarcinoma: correlation of thin-section CT findings with histologic prognostic factors and survival. Radiology. 2001;220(3):803–9.
5. Kim EA, Johkoh T, Lee KS, et al. Quantification of ground-glass opacity on high-resolution CT of small peripheral adenocarcinoma of the lung: pathologic and prognostic implications. AJR Am J Roentgenol. 2001;177(6):1417–22.
6. Kuriyama K, Seto M, Kasugai T, et al. Ground-glass opacity on thin-section CT: value in differentiating subtypes of adenocarcinoma of the lung. AJR Am J Roentgenol. 1999;173(2):465–9.
7. Nakata M, Saeki H, Takata I, et al. Focal ground-glass opacity detected by low-dose helical CT. Chest. 2002;121(5):1464–7.
8. Cheran SK, Nielsen ND, Patz Jr EF. False-negative findings for primary lung tumors on FDG positron emission tomography: staging and prognostic implications. AJR Am J Roentgenol. 2004;182(5):1129–32.
9. Lee KS, Jeong YJ, Han J, Kim BT, Kim H, Kwon OJ. T1 non-small cell lung cancer: imaging and histopathologic findings and their prognostic implications. Radiographics. 2004;24(6):1617–36; discussion 1632–6.
10. Lindell RM, Hartman TE, Swensen SJ, et al. Lung cancer screening experience: a retrospective review of PET in 22 non-small cell lung carcinomas detected on screening chest CT in a high-risk population. AJR Am J Roentgenol. 2005;185(1):126–31.
11. Travis WD, Garg K, Franklin WA, et al. Evolving concepts in the pathology and computed tomography imaging of lung adenocarcinoma and bronchioloalveolar carcinoma. J Clin Oncol. 2005;23(14):3279–87.
12. Patsios D, Roberts HC, Paul NS, et al. Pictorial review of the many faces of bronchioloalveolar cell carcinoma. Br J Radiol. 2007;80(960):1015–23.
13. Gaeta M, Caruso R, Blandino A, Bartiromo G, Scribano E, Pandolfo I. Radiolucencies and cavitation in bronchioloalveolar carcinoma: CT-pathologic correlation. Eur Radiol. 1999;9(1):55–9.
14. Weisbrod GL, Towers MJ, Chamberlain DW, Herman SJ, Matzinger FR. Thin-walled cystic lesions in bronchioalveolar carcinoma. Radiology. 1992;185(2):401–5.
15. Gandara DR, Aberle D, Lau D, et al. Radiographic imaging of bronchioloalveolar carcinoma: screening, patterns of presentation and response assessment. J Thorac Oncol. 2006;1(9 Suppl):S20–6.
16. Jung JI, Kim H, Park SH, et al. CT differentiation of pneumonic-type bronchioloalveolar cell carcinoma and infectious pneumonia. Br J Radiol. 2001;74(882):490–4.

17. Aquino SL, Chiles C, Halford P. Distinction of consolidative bronchioloalveolar carcinoma from pneumonia: do CT criteria work? AJR Am J Roentgenol. 1998;171(2):359–63.
18. Shah RM, Friedman AC. CT angiogram sign: incidence and significance in lobar consolidations evaluated by contrast-enhanced CT. AJR Am J Roentgenol. 1998;170(3):719–21.
19. Mountain CF. Revisions in the International System for Staging Lung Cancer. Chest. 1997;111(6): 1710–7.
20. Cascade PN, Gross BH, Kazerooni EA, et al. Variability in the detection of enlarged mediastinal lymph nodes in staging lung cancer: a comparison of contrast-enhanced and unenhanced CT. AJR Am J Roentgenol. 1998;170(4):927–31.
21. Haramati LB, Cartagena AM, Austin JH. CT evaluation of mediastinal lymphadenopathy: noncontrast 5 mm vs postcontrast 10 mm sections. J Comput Assist Tomogr. 1995;19(3):375–8.
22. Patz EJ, Erasmus J, McAdams H, et al. Lung cancer staging and management: comparison of contrast-enhanced and nonenhanced helical CT of the thorax. Radiology. 1999;212(1):56–60.
23. Munden RF, Swisher SS, Stevens CW, Stewart DJ. Imaging of the patient with non-small cell lung cancer. Radiology. 2005;237(3):803–18.
24. Pearlberg JL, Sandler MA, Beute GH, Lewis Jr JW, Madrazo BL. Limitations of CT in evaluation of neoplasms involving chest wall. J Comput Assist Tomogr. 1987;11(2):290–3.
25. Pennes DR, Glazer GM, Wimbish KJ, Gross BH, Long RW, Orringer MB. Chest wall invasion by lung cancer: limitations of CT evaluation. AJR Am J Roentgenol. 1985;144(3):507–11.
26. Glazer HS, Duncan-Meyer J, Aronberg DJ, Moran JF, Levitt RG, Sagel SS. Pleural and chest wall invasion in bronchogenic carcinoma: CT evaluation. Radiology. 1985;157(1):191–4.
27. Higashino T, Ohno Y, Takenaka D, et al. Thin-section multiplanar reformats from multidetector-row CT data: utility for assessment of regional tumor extent in non-small cell lung cancer. Eur J Radiol. 2005;56(1):48–55.
28. Bruzzi JF, Komaki R, Walsh GL, et al. Imaging of non-small cell lung cancer of the superior sulcus: part 2: initial staging and assessment of resectability and therapeutic response. Radiographics. 2008; 28(2):561–72.
29. Akata S, Kajiwara N, Park J, et al. Evaluation of chest wall invasion by lung cancer using respiratory dynamic MRI. J Med Imaging Radiat Oncol. 2008; 52(1):36–9.
30. Sakai S, Murayama S, Murakami J, Hashiguchi N, Masuda K. Bronchogenic carcinoma invasion of the chest wall: evaluation with dynamic cine MRI during breathing. J Comput Assist Tomogr. 1997;21(4): 595–600.
31. Seo JS, Kim YJ, Choi BW, Choe KO. Usefulness of magnetic resonance imaging for evaluation of cardiovascular invasion: evaluation of sliding motion between thoracic mass and adjacent structures on cine MR images. J Magn Reson Imaging. 2005; 22(2):234–41.
32. Bandi V, Lunn W, Ernst A, Eberhardt R, Hoffmann H, Herth FJ. Ultrasound vs. CT in detecting chest wall invasion by tumor: a prospective study. Chest. 2008;133(4):881–6.
33. Suzuki N, Saitoh T, Kitamura S. Tumor invasion of the chest wall in lung cancer: diagnosis with US. Radiology. 1993;187(1):39–42.
34. Schroder C, Schonhofer B, Vogel B. Transesophageal echographic determination of aortic invasion by lung cancer. Chest. 2005;127(2):438–42.
35. Varadarajulu S, Schmulewitz N, Wildi SM, et al. Accuracy of EUS in staging of T4 lung cancer. Gastrointest Endosc. 2004;59(3):345–8.
36. Lardinois D, Weder W, Hany TF, et al. Staging of non-small-cell lung cancer with integrated positron-emission tomography and computed tomography. N Engl J Med. 2003;348(25):2500–7.
37. Downey RJ, Akhurst T, Gonen M, et al. Preoperative F-18 fluorodeoxyglucose-positron emission tomography maximal standardized uptake value predicts survival after lung cancer resection. J Clin Oncol. 2004;22(16):3255–60.
38. Downey RJ, Akhurst T, Gonen M, Park B, Rusch V. Fluorine-18 fluorodeoxyglucose positron emission tomographic maximal standardized uptake value predicts survival independent of clinical but not pathologic TNM staging of resected non-small cell lung cancer. J Thorac Cardiovasc Surg. 2007; 133(6):1419–27.
39. Goodgame B, Pillot GA, Yang Z, et al. Prognostic value of preoperative positron emission tomography in resected stage I non-small cell lung cancer. J Thorac Oncol. 2008;3(2):130–4.
40. Higashi K, Ueda Y, Arisaka Y, et al. 18F-FDG uptake as a biologic prognostic factor for recurrence in patients with surgically resected non-small cell lung cancer. J Nucl Med. 2002;43(1):39–45.
41. Sasaki R, Komaki R, Macapinlac H, et al. [18F]fluorodeoxyglucose uptake by positron emission tomography predicts outcome of non-small-cell lung cancer. J Clin Oncol. 2005;23(6):1136–43.
42. Vansteenkiste JF, Stroobants SG, Dupont PJ, et al. Prognostic importance of the standardized uptake value on (18)F-fluoro-2-deoxy-glucose-positron emission tomography scan in non-small-cell lung cancer: an analysis of 125 cases. Leuven Lung Cancer Group. J Clin Oncol. 1999;17(10):3201–6.
43. Berghmans T, Dusart M, Paesmans M, et al. Primary tumor standardized uptake value (SUVmax) measured on fluorodeoxyglucose positron emission tomography (FDG-PET) is of prognostic value for survival in non-small cell lung cancer (NSCLC): a systematic review and meta-analysis (MA) by the European Lung Cancer Working Party for the IASLC Lung Cancer Staging Project. J Thorac Oncol. 2008;3(1):6–12.

44. Rusch VW, Asamura H, Watanabe H, et al. The IASLC lung cancer staging project: a proposal for a new international lymph node map in the forthcoming seventh edition of the TNM classification for lung cancer. J Thorac Oncol. 2009;4(5):568–77.
45. Cerfolio RJ, Bryant AS. Distribution and likelihood of lymph node metastasis based on the lobar location of nonsmall-cell lung cancer. Ann Thorac Surg. 2006;81(6):1969–73; discussion 1973.
46. Watanabe S, Suzuki K, Asamura H. Superior and basal segment lung cancers in the lower lobe have different lymph node metastatic pathways and prognosis. Ann Thorac Surg. 2008;85(3):1026–31.
47. Glazer GM, Gross BH, Quint LE, Francis IR, Bookstein FL, Orringer MB. Normal mediastinal lymph nodes: number and size according to American Thoracic Society mapping. AJR Am J Roentgenol. 1985;144(2):261–5.
48. de Langen AJ, Raijmakers P, Riphagen I, Paul MA, Hoekstra OS. The size of mediastinal lymph nodes and its relation with metastatic involvement: a meta-analysis. Eur J Cardiothorac Surg. 2006;29(1):26–9.
49. Silvestri GA, Gould MK, Margolis ML, et al. Noninvasive staging of non-small cell lung cancer: ACCP evidenced-based clinical practice guidelines (2nd edition). Chest. 2007;132(3 Suppl):178S–201.
50. Gould MK, Kuschner WG, Rydzak CE, et al. Test performance of positron emission tomography and computed tomography for mediastinal staging in patients with non-small-cell lung cancer: a meta-analysis. Ann Intern Med. 2003;139(11):879–92.
51. van Tinteren H, Hoekstra O, Smit E, et al. Effectiveness of positron emission tomography in the preoperative assessment of patients with suspected non-small cell lung cancer: the PLUS multicentre randomised trial. Lancet. 2002;359(9315):1388–93.
52. Reed CE, Harpole DH, Posther KE, et al. Results of the American College of Surgeons Oncology Group Z0050 trial: the utility of positron emission tomography in staging potentially operable non-small cell lung cancer. J Thorac Cardiovasc Surg. 2003;126(6):1943–51.
53. Kozower BD, Meyers BF, Reed CE, Jones DR, Decker PA, Putnam JB Jr. Does positron emission tomography prevent nontherapeutic pulmonary resections for clinical stage IA lung cancer? Ann Thorac Surg. 2008;85(4):1166–9; discussion 1169–70.
54. Kelly RF, Tran T, Holmstrom A, Murar J, Segurola Jr RJ. Accuracy and cost-effectiveness of [18F]-2-fluoro-deoxy-D-glucose-positron emission tomography scan in potentially resectable non-small cell lung cancer. Chest. 2004;125(4):1413–23.
55. Bryant AS, Cerfolio RJ, Klemm KM, Ojha B. Maximum standard uptake value of mediastinal lymph nodes on integrated FDG-PET-CT predicts pathology in patients with non-small cell lung cancer. Ann Thorac Surg. 2006;82(2):417–22; discussion 422–3.
56. Nomori H, Watanabe K, Ohtsuka T, Naruke T, Suemasu K, Uno K. The size of metastatic foci and lymph nodes yielding false-negative and false-positive lymph node staging with positron emission tomography in patients with lung cancer. J Thorac Cardiovasc Surg. 2004;127(4):1087–92.
57. Cerfolio RJ, Bryant AS. Ratio of the maximum standardized uptake value on FDG-PET of the mediastinal (N2) lymph nodes to the primary tumor may be a universal predictor of nodal malignancy in patients with nonsmall-cell lung cancer. Ann Thorac Surg. 2007;83(5):1826–9; discussion 1829–30.
58. Lee PC, Port JL, Korst RJ, Liss Y, Meherally DN, Altorki NK. Risk factors for occult mediastinal metastases in clinical stage I non-small cell lung cancer. Ann Thorac Surg. 2007;84(1):177–81.
59. Cerfolio RJ, Bryant AS, Eloubeidi MA. Routine mediastinoscopy and esophageal ultrasound fine-needle aspiration in patients with non-small cell lung cancer who are clinically N2 negative: a prospective study. Chest. 2006;130(6):1791–5.
60. Hishida T, Yoshida J, Nishimura M, Nishiwaki Y, Nagai K. Problems in the current diagnostic standards of clinical N1 non-small cell lung cancer. Thorax. 2008;63(6):526–31.
61. Bryant AS, Cerfolio RJ. The clinical stage of non-small cell lung cancer as assessed by means of fluorodeoxyglucose-positron emission tomographic/computed tomographic scanning is less accurate in cigarette smokers. J Thorac Cardiovasc Surg. 2006;132(6):1363–8.
62. Antoch G, Stattaus J, Nemat AT, et al. Non-small cell lung cancer: dual-modality PET/CT in preoperative staging. Radiology. 2003;229(2):526–33.
63. Aquino SL, Asmuth JC, Alpert NM, Halpern EF, Fischman AJ. Improved radiologic staging of lung cancer with 2-[18F]-fluoro-2-deoxy-D-glucose-positron emission tomography and computed tomography registration. J Comput Assist Tomogr. 2003;27(4):479–84.
64. Cerfolio RJ, Ojha B, Bryant AS, Raghuveer V, Mountz JM, Bartolucci AA. The accuracy of integrated PET-CT compared with dedicated PET alone for the staging of patients with nonsmall cell lung cancer. Ann Thorac Surg. 2004;78(3):1017–23; discussion 1017–23.
65. Goerres GW, Kamel E, Seifert B, et al. Accuracy of image coregistration of pulmonary lesions in patients with non-small cell lung cancer using an integrated PET/CT system. J Nucl Med. 2002;43(11):1469–75.
66. Schlemmer HP, Schafer J, Pfannenberg C, et al. Fast whole-body assessment of metastatic disease using a novel magnetic resonance imaging system: initial experiences. Invest Radiol. 2005;40(2):64–71.
67. Plathow C, Aschoff P, Lichy MP, et al. Positron emission tomography/computed tomography and whole-body magnetic resonance imaging in staging of advanced nonsmall cell lung cancer–initial results. Invest Radiol. 2008;43(5):290–7.

68. Yi CA, Shin KM, Lee KS, et al. Non-small cell lung cancer staging: efficacy comparison of integrated PET/CT versus 3.0-T whole-body MR imaging. Radiology. 2008;248(2):632–42.
69. Ohno Y, Koyama H, Nogami M, et al. Whole-body MR imaging vs. FDG-PET: comparison of accuracy of M-stage diagnosis for lung cancer patients. J Magn Reson Imaging. 2007;26(3):498–509.
70. Ohno Y, Koyama H, Yoshikawa T, et al. N stage disease in patients with non-small cell lung cancer: efficacy of quantitative and qualitative assessment with STIR turbo spin-echo imaging, diffusion-weighted MR imaging, and fluorodeoxyglucose PET/CT. Radiology. 2011;261(2):605–15.
71. Usuda K, Zhao XT, Sagawa M, et al. Diffusion-weighted imaging is superior to positron emission tomography in the detection and nodal assessment of lung cancers. Ann Thorac Surg. 2011;91(6): 1689–95.
72. Pauls S, Schmidt SA, Juchems MS, et al. Diffusion-weighted MR imaging in comparison to integrated [(18)F]-FDG PET/CT for N-staging in patients with lung cancer. Eur J Radiol. 2012;81(1):178–82.
73. Baysal T, Mutlu DY, Yologlu S. Diffusion-weighted magnetic resonance imaging in differentiation of postobstructive consolidation from central lung carcinoma. Magn Reson Imaging. 2009;27(10): 1447–54.
74. Silvestri G, Littenberg B, Colice G. The clinical evaluation for detecting metastatic lung cancer: a meta-analysis. Am J Respir Crit Care Med. 1995;152(1):225–30.
75. Silvestri GA, Tanoue LT, Margolis ML, Barker J, Detterbeck F, American College of Chest Physicians. The noninvasive staging of non-small cell lung cancer: the guidelines. Chest. 2003;123(1 Suppl): 147S–56.
76. Ohno Y, Koyama H, Onishi Y, et al. Non-small cell lung cancer: whole-body MR examination for M-stage assessment–utility for whole-body diffusion-weighted imaging compared with integrated FDG PET/CT. Radiology. 2008;248(2): 643–54.
77. Heffner JE, Klein JS. Recent advances in the diagnosis and management of malignant pleural effusions. Mayo Clin Proc. 2008;83(2):235–50.
78. American Thoracic Society. Management of malignant pleural effusions. Am J Respir Crit Care Med. 2000;162(5):1987–2001.
79. Erasmus JJ, McAdams HP, Rossi SE, Goodman PC, Coleman RE, Patz EF. FDG PET of pleural effusions in patients with non-small cell lung cancer. AJR Am J Roentgenol. 2000;175(1):245–9.
80. Gupta NC, Rogers JS, Graeber GM, et al. Clinical role of F-18 fluorodeoxyglucose positron emission tomography imaging in patients with lung cancer and suspected malignant pleural effusion. Chest. 2002;122(6):1918–24.
81. Boland GW, Lee MJ, Gazelle GS, Halpern EF, McNicholas MM, Mueller PR. Characterization of adrenal masses using unenhanced CT: an analysis of the CT literature. AJR Am J Roentgenol. 1998; 171(1):201–4.
82. Boland GW, Hahn PF, Pena C, Mueller PR. Adrenal masses: characterization with delayed contrast-enhanced CT. Radiology. 1997;202(3):693–6.
83. Pena CS, Boland GW, Hahn PF, Lee MJ, Mueller PR. Characterization of indeterminate (lipid-poor) adrenal masses: use of washout characteristics at contrast-enhanced CT. Radiology. 2000;217(3): 798–802.
84. Ho LM, Paulson EK, Brady MJ, Wong TZ, Schindera ST. Lipid-poor adenomas on unenhanced CT: does histogram analysis increase sensitivity compared with a mean attenuation threshold? AJR Am J Roentgenol. 2008;191(1):234–8.
85. Jhaveri KS, Wong F, Ghai S, Haider MA. Comparison of CT histogram analysis and chemical shift MRI in the characterization of indeterminate adrenal nodules. AJR Am J Roentgenol. 2006;187(5):1303–8.
86. Remer EM, Motta-Ramirez GA, Shepardson LB, Hamrahian AH, Herts BR. CT histogram analysis in pathologically proven adrenal masses. AJR Am J Roentgenol. 2006;187(1):191–6.
87. Jhaveri KS, Lad SV, Haider MA. Computed tomographic histogram analysis in the diagnosis of lipid-poor adenomas: comparison to adrenal washout computed tomography. J Comput Assist Tomogr. 2007;31(4):513–8.
88. Heinz-Peer G, Honigschnabi S, Schneider B, Niederle B, Kaserer K, Lechner G. Characterization of adrenal masses using MR imaging with histopathologic correlation. AJR Am J Roentgenol. 1999;173(1):15–22.
89. Korobkin M, Giordano TJ, Brodeur FJ, et al. Adrenal adenomas: relationship between histologic lipid and CT and MR findings. Radiology. 1996;200(3):743–7.
90. Outwater EK, Siegelman ES, Huang AB, Birnbaum BA. Adrenal masses: correlation between CT attenuation value and chemical shift ratio at MR imaging with in-phase and opposed-phase sequences. Radiology. 1996;200(3):749–52.
91. Erasmus J, Patz Jr E, McAdams H, et al. Evaluation of adrenal masses in patients with bronchogenic carcinoma using 18F-fluorodeoxyglucose positron emission tomography. AJR Am J Roentgenol. 1997;168(5):1357–60.
92. Gupta NC, Graeber GM, Tamim WJ, Rogers JS, Irisari L, Bishop HA. Clinical utility of PET-FDG imaging in differentiation of benign from malignant adrenal masses in lung cancer. Clin Lung Cancer. 2001;3(1):59–64.
93. Vikram R, Yeung HD, Macapinlac HA, Iyer RB. Utility of PET/CT in differentiating benign from malignant adrenal nodules in patients with cancer. AJR Am J Roentgenol. 2008;191(5):1545–51.
94. Yun M, Kim W, Alnafisi N, Lacorte L, Jang S, Alavi A. 18F-FDG PET in characterizing adrenal lesions detected on CT or MRI. J Nucl Med. 2001; 42(12):1795–9.

95. Kagohashi K, Satoh H, Ishikawa H, Ohtsuka M, Sekizawa K. Liver metastasis at the time of initial diagnosis of lung cancer. Med Oncol. 2003;20(1): 25–8.
96. Delbeke D, Martin WH, Sandler MP, Chapman WC, Wright JK Jr, Pinson CW. Evaluation of benign vs malignant hepatic lesions with positron emission tomography. Arch Surg. 1998;133(5):510–5; discussion 515–6.
97. Little AG, Stitik FP. Clinical staging of patients with non-small cell lung cancer. Chest. 1990;97(6):1431–8.
98. Cheran SK, Herndon 2nd JE, Patz Jr EF. Comparison of whole-body FDG-PET to bone scan for detection of bone metastases in patients with a new diagnosis of lung cancer. Lung Cancer. 2004;44(3):317–25.
99. Gayed I, Vu T, Johnson M, Macapinlac H, Podoloff D. Comparison of bone and 2-deoxy-2-[18F]fluoro-D-glucose positron emission tomography in the evaluation of bony metastases in lung cancer. Mol Imaging Biol. 2003;5(1):26–31.
100. Hsia TC, Shen YY, Yen RF, Kao CH, Changlai SP. Comparing whole body 18F-2-deoxyglucose positron emission tomography and technetium-99m methylene diophosphate bone scan to detect bone metastases in patients with non-small cell lung cancer. Neoplasma. 2002;49(4):267–71.
101. Davis PC, Hudgins PA, Peterman SB, Hoffman Jr JC. Diagnosis of cerebral metastases: double-dose delayed CT vs contrast-enhanced MR imaging. AJNR Am J Neuroradiol. 1991;12(2):293–300.
102. Mujoomdar A, Austin JH, Malhotra R, et al. Clinical predictors of metastatic disease to the brain from non-small cell lung carcinoma: primary tumor size, cell type, and lymph node metastases. Radiology. 2007;242(3):882–8.
103. Cole JFH, Thomas JE, Wilcox AB, Halford 3rd HH. Cerebral imaging in the asymptomatic preoperative bronchogenic carcinoma patient: is it worthwhile? Ann Thorac Surg. 1994;57(4):838–40.
104. Colice G, Birkmeyer J, Black W, Littenberg B, Silvestri G. Cost-effectiveness of head CT in patients with lung cancer without clinical evidence of metastases. Chest. 1995;108(5):1264–71.
105. Ferrigno D, Buccheri G. Cranial computed tomography as a part of the initial staging procedures for patients with non-small cell lung cancer. Chest. 1994;106(4):1025–9.
106. Mintz BJ, Turhim S, Alexander S, Yang WC, Shanzer S. Intracranial metastases in the initial staging of bronchogenic carcinoma. Chest. 1984;86: 850–3.
107. Rohren EM, Provenzale JM, Barboriak DP, Coleman RE. Screening for cerebral metastases with FDG PET in patients undergoing whole-body staging of non-central nervous system malignancy. Radiology. 2003;226(1):181–7.
108. Wang J, Wu N, Cham MD, Song Y. Tumor response in patients with advanced non-small cell lung cancer: perfusion CT evaluation of chemotherapy and radiation therapy. AJR Am J Roentgenol. 2009; 193(4):1090–6.
109. Fraioli F, Anzidei M, Zaccagna F, et al. Whole-tumor perfusion CT in patients with advanced lung adenocarcinoma treated with conventional and anti-angiogenetic chemotherapy: initial experience. Radiology. 2011;259(2):574–82.
110. Sohn HJ, Yang YJ, Ryu JS, et al. [18F] Fluorothymidine positron emission tomography before and 7 days after gefitinib treatment predicts response in patients with advanced adenocarcinoma of the lung. Clin Cancer Res. 2008;14(22): 7423–9.
111. Everitt S, Hicks RJ, Ball D, et al. Imaging cellular proliferation during chemo-radiotherapy: a pilot study of serial 18F-FLT positron emission tomography/computed tomography imaging for non-small-cell lung cancer. Int J Radiat Oncol Biol Phys. 2009;75(4):1098–104.
112. Yamamoto Y, Nishiyama Y, Ishikawa S, et al. Correlation of 18F-FLT and 18F-FDG uptake on PET with Ki-67 immunohistochemistry in non-small cell lung cancer. Eur J Nucl Med Mol Imaging. 2007;34(10):1610–6.
113. Yang W, Zhang Y, Fu Z, et al. Imaging of proliferation with 18F-FLT PET/CT versus 18F-FDG PET/CT in non-small-cell lung cancer. Eur J Nucl Med Mol Imaging. 2010;37(7):1291–9.
114. Dittmann H, Dohmen BM, Paulsen F, et al. [18F] FLT PET for diagnosis and staging of thoracic tumours. Eur J Nucl Med Mol Imaging. 2003;30(10): 1407–12.
115. Krohn KA, Link JM, Mason RP. Molecular imaging of hypoxia. J Nucl Med. 2008;49 Suppl 2:129S–48.
116. Rajendran JG, Schwartz DL, O'Sullivan J, et al. Tumor hypoxia imaging with [F-18] fluoromisonidazole positron emission tomography in head and neck cancer. Clin Cancer Res. 2006;12(18): 5435–41.